Available online at www.sciencedirect.com

SciVerse ScienceDirect

Ceramics International 39 (2013) 865–869

CERAMICS INTERNATIONAL

www.elsevier.com/locate/ceramint

Short communication

Effects of debinding atmosphere on the microstructure and sintering densification of nickel ferrite

Yuqiang Tao, Zhiyou Li, Kechao Zhou*

State Key Laboratory of Powder Metallurgy, Central South University, Changsha 410083, China

Received 13 April 2012; received in revised form 29 May 2012; accepted 1 June 2012
Available online 13 June 2012

Abstract

Microsized nickel ferrite ($NiFe_2O_4$) powders were synthesized by molten salt synthesis in KCl flux using Fe_2O_3 and NiO as raw materials. The binder burnout process of the compact containing 1.2 wt% poly vinyl alcohol was performed in air and N_2 atmospheres, followed by sintering in N_2 atmosphere. The effects of debinding atmosphere on the microstructure and sintering densification of $NiFe_2O_4$ were studied using X-ray diffraction (XRD), scanning electron microscopy (SEM), energy-dispersive X-ray analysis (EDS) and X-ray photoelectron spectroscopy (XPS). Metallic Ni particles were found uniformly distributed on the surface of $NiFe_2O_4$ particles debound in N_2 atmosphere. The densifications of the samples sintered at 1150 °C and 1300 °C were 90.7% and 97.2% respectively when the binder burnout process was performed in N_2 atmosphere. They increased by 15% and 6.7% respectively compared with those debound in air. The temperature for the debound sample to reach a densification of 90% was 150 °C lower in N_2 atmosphere than that in air. Also the average grain size of $NiFe_2O_4$ and Fe/Ni ratio in $NiFe_2O_4$ phase of the sintered samples debound in N_2 atmosphere showed a significant increase, compared with those debound in air.

Keywords: A. Sintering; A. Grain growth; B. Microstructure-Prefiring; D. Ferrites

1. Introduction

The development of inert anode for the production of aluminum in Hall–Heroult cells has attracted a lot of attention since the middle of 1980s, because instead of greenhouse gases, it produces O_2 only, which is apparently environment-friendly, and in the meanwhile it is non-consumable in electrolysis process [1–3]. Owing to its high corrosion resistance in cryolite molten salt, nickel ferrite ($NiFe_2O_4$) has been widely used as the main component of inert anode materials. Pilot scale electrolysis experiments with $NiFe_2O_4$ based cermet inert anode (Cu/Ni as the metallic phase) have been carried out for 25 days in Reynolds' Manufacturing Technology Laboratory [4] and 28 days in Aluminum Corp. of China Ltd. [5]. Many researches have revealed that Ni was anodically dissolvable in electrolysis [6,7]. However, the Ni content in $NiFe_2O_4$ based cermet was always higher than the theoretical value [8,9]. Weyand [8] thought the increase of Ni content was caused by the exchange reaction between Cu, NiO and $NiFe_2O_4$, while Olsen and Thonstad [9] considered it as a result of the carbothermic reduction of the oxide phases by carbon residues during sintering. Additionally, the densification of the inert anode materials plays a crucial role in the corrosion resistance of the inert anode [10,11]. The high densification is in favor of increasing the electrical conductivity and improving the corrosion resistance. Many measures have been used to improve the sintering densification of the inert anode, such as doping [12,13] and adjusting the sintering atmosphere [14,15]. However, to the best of our knowledge, little literature has been reported about the microstructure of the as-debound $NiFe_2O_4$ particle and the effect of debinding atmosphere on the sintering densification of $NiFe_2O_4$.

In this paper, $NiFe_2O_4$ powders were synthesized by molten salt synthesis (MSS), and the binder burnout process of the $NiFe_2O_4$ compacts containing 1.2 wt% poly vinyl alcohol (PVA) was performed in air and N_2

*Corresponding author. Tel.: +86 731 88836418; fax: +86 731 88830464.
E-mail address: zhoukc2@csu.edu.cn (K. Zhou).

0272-8842/$36.00
http://dx.doi.org/10.1016/j.ceramint.2012.06.006

atmospheres followed by sintering process in N_2 atmosphere. The effects of debinding atmosphere on the microstructure and sintering densification of $NiFe_2O_4$ were studied.

2. Experimental

Analytical grade NiO (77.64 wt% Ni, <10 μm, Jinchuan Group Ltd., China), Fe_2O_3 (99.60%, 0.75 μm, JFE Chemical Co., Japan) and KCl (99.5%, Tianjin Damao Chemical Reagent Factory, China) powders were mixed in a molar ratio of 1:1:4 and ball-milled for 8 h in zirconia media using ethanol as solvent. The mixture was heated at 1200 °C for 6 h in air, and then cooled down at a rate of 0.5 °C/min to room temperature. The salt was washed away with hot deionized water several times until the water became Cl^- free, and the remaining powders were dried overnight at 80 °C. Compacts containing 1.2 wt% PVA were prepared by pressing at 100 MPa into a pellet 12 mm in diameter and 4 mm in thickness. The binder burnout process was performed at 600 °C in air and N_2 atmospheres respectively, and followed by sintering at 1150 °C and 1300 °C for 4 h in N_2 atmosphere. The purity of the N_2 gas was 99.99%.

The phase compositions were characterized using X-ray diffraction (XRD) (Rigaku D/max 2550VB, Rigaku Corporation, Tokyo, Japan) with Cu Kα radiation ($\lambda = 0.15406$ nm) at a scan rate of 4°/min. The microstructures were observed using FEI Quanta-200 scanning electron microscopy (SEM) and Hitachi S-4800 field emission scanning electron microscopy (FESEM). The element contents in different phases were analyzed by X-ray energy-dispersive spectroscopy (EDS) (EDX-GENESIS 60S, EDAX Company of America, America). The content of residual carbon in the debound compact was measured using a LECO CS-600C/S analyzer. The Ni and Fe charges of the debound compacts were studied by X-ray photoelectron spectroscopy (XPS). XPS analyses were carried out in a Thermo Fisher Scientific probe with Al Kα radiations. The reporting peaks were corrected with respect to the C 1 s peak positioned at 284.6 eV. The spectrums were fitted with XPSPEAK41 program. The porosities of the samples were obtained using Q550 quantitative image analyzer (Leica Corporation, Germany), and the densification was equal to one minus the porosity. The SEM photographs of the etched samples were used to measure the grain size of $NiFe_2O_4$ using Image-pro plus 6.0 (Media Cybernetics Inc., USA).

3. Results and discussion

3.1. Microstructure of the synthesized powder

Fig. 1 (a) shows the XRD pattern of the synthesized powder. The diffraction peaks were well indexed to the $NiFe_2O_4$ crystal structure (JCPDS card number: 54-0964). The EDS results revealed that the Fe/Ni atomic ratio in $NiFe_2O_4$ phase was about 2.05, which was almost in agreement with the stoichiometric ratio of $NiFe_2O_4$. Considering this result with the XRD pattern, the synthesized powder was mainly composed of $NiFe_2O_4$, with a very low content of NiO. Fig. 1(b) and (c) shows the micrographs of the synthesized powder. The particle size was in the range from 1 μm to 10 μm. The facets of the particles were flat, as shown in Fig. 1(c). Some particles had pronounced octahedral morphology.

3.2. Microstructures of the debound compacts

Fig. 2(a) and (b) shows the micrographs of the as-debound $NiFe_2O_4$ particles. The morphology of the $NiFe_2O_4$ particle debound in air was similar to that of the synthesized powder, both of which contained a flat surface, as shown in Figs. 1(c) and 2(a). However, some small particles with a size of about 0.1 μm were found distributed uniformly on the surface of the $NiFe_2O_4$ particle debound in N_2 atmosphere, as shown in Fig. 2(b) and (c).

Fig. 2(d) shows the XRD patterns of the debound compacts. Comparing Fig. 2(d) with Fig. 1(a), it was found that the compact debound in air was mainly composed of $NiFe_2O_4$ phase, same as the synthesized powder, whereas Ni phase was found in the compact debound in N_2 atmosphere. The small particles were probably metallic Ni.

In order to further identify the small particles, the debound compacts were also characterized using XPS, and the results are shown in Fig. 3. The results showed

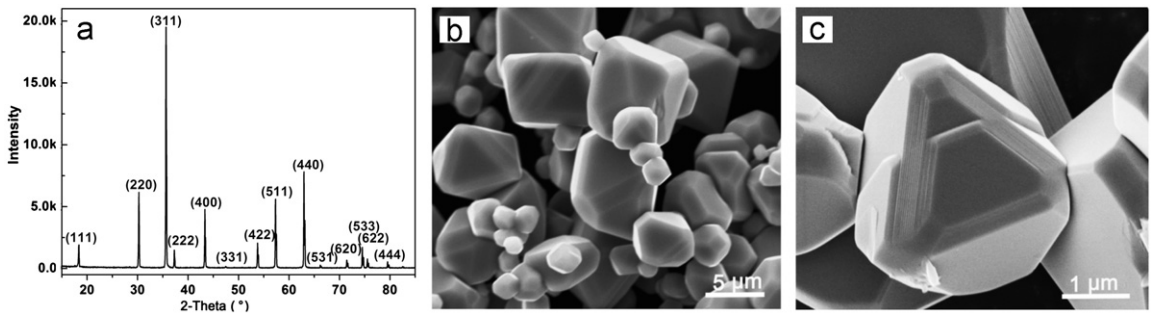

Fig. 1. (a) XRD pattern, (b) SEM image and (c) FESEM image of the synthesized $NiFe_2O_4$ powder.

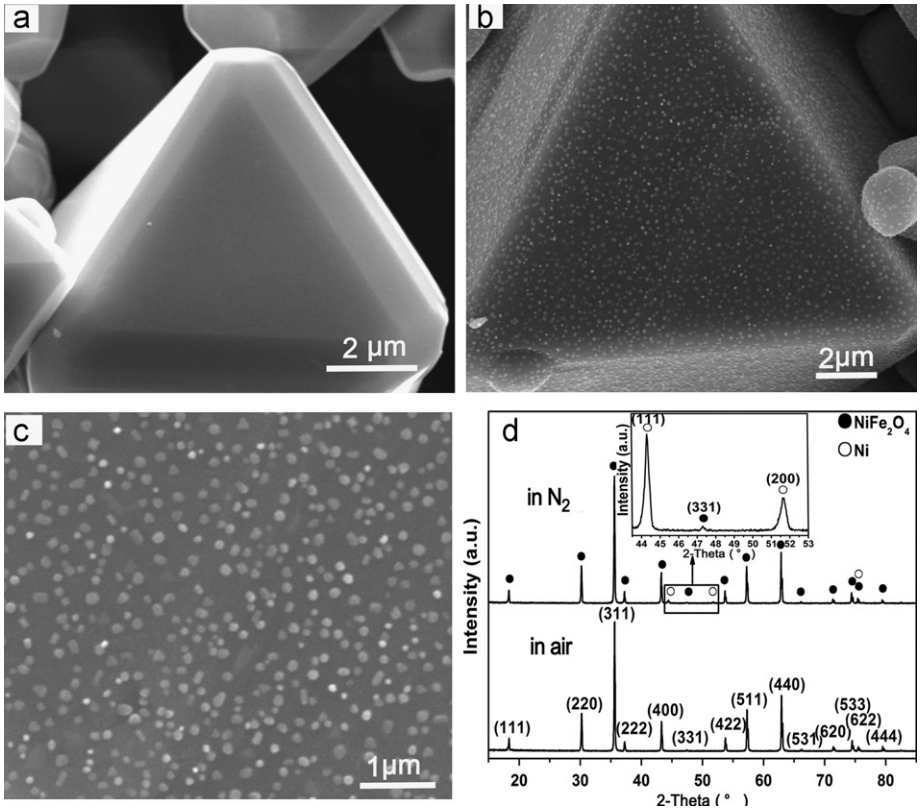

Fig. 2. (a), (b), (c) SEM images and (d) XRD patterns of the debound compacts. (a) was debound in air; and (b) and (c) were debound in N_2 atmospheres; (c) was the higher magnification of (b).

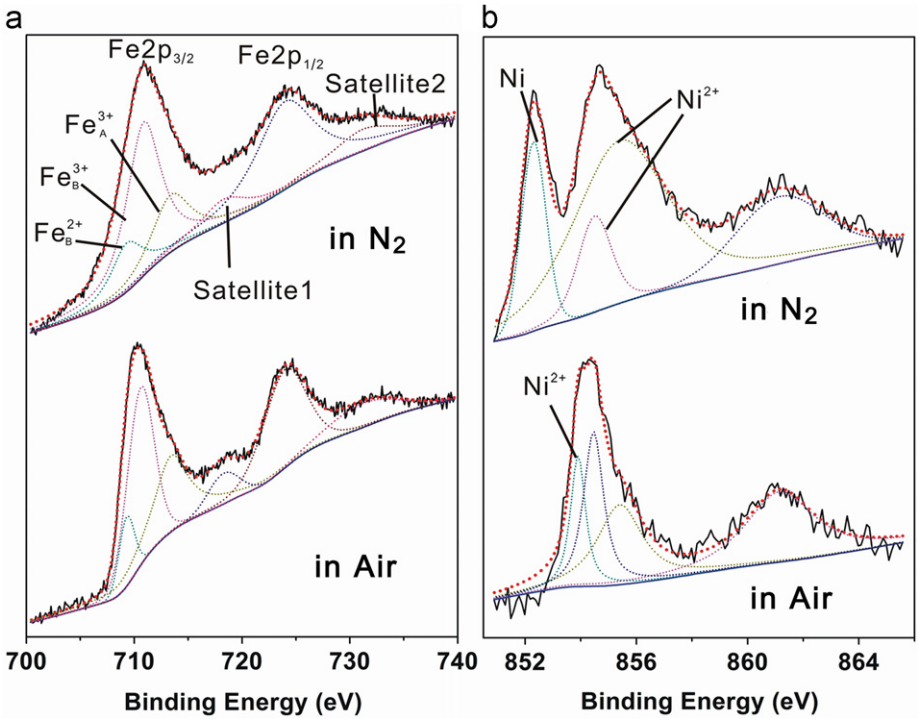

Fig. 3. XPS spectra of (a) Fe 2p and (b) Ni 2p 3/2 of the debound compacts. Fe_B^{2+} is the Fe^{2+} cation located in the octahedral interstices of $NiFe_2O_4$. Fe_A^{3+} and Fe_B^{3+} are the Fe^{3+} cations located in the tetrahedral and octahedral interstices of $NiFe_2O_4$ respectively.

that Fe^0 was free in both the debound compacts, and Ni^0 was just found in the compact debound in N_2 atmosphere. Considering this result with Fig. 2(d), the small particles should be metallic Ni, instead of Ni–Fe alloy [16]. Additionally, satellite 1 of the compact debound in N_2 atmosphere was less obvious than that debound in air, as shown

in Fig. 3(a). The weaker the strength of satellite 1 was, the more Fe^{2+} existed [17]. Therefore, the Fe^{2+} of $NiFe_2O_4$ debound in N_2 atmosphere was more than that debound in air. Besides Ni^{2+} from $NiFe_2O_4$ (855.4 eV), both compacts also contained Ni^{2+} from NiO, whose binding energy is about 853.8 eV or 854.3 eV [18], as shown in Fig. 3(b).

3.3. Sintering densification

Fig. 4 shows the micrographs of the samples sintered at 1150 °C and 1300 °C. Both NiO and $NiFe_2O_4$ phases were found in all samples. Metallic phase was only found in the samples debound in N_2 atmosphere. The pores of the samples debound in N_2 atmosphere were less compared with those debound in air. A lot of interconnected pores were found in the 1150 °C sintered sample when binder burnout process was performed in air, while for the sample performed in N_2 atmosphere, pores were mostly isolated ones.

The densifications, grain sizes of $NiFe_2O_4$, and Fe/Ni atomic ratios in $NiFe_2O_4$ phase of the sintered samples are shown in Table 1. The densifications of the samples debound in N_2 atmosphere increased by 15% and 6.7% , compared with those debound in air when sintered at 1150 °C and 1300 °C. With the increase of the sintering temperature, the effect of debinding atmosphere on densification decreased. The temperature for the debound sample to reach a densification of 90% was 150 °C lower in N_2 atmosphere than that in air. The grain sizes of $NiFe_2O_4$ in the samples debound in N_2 atmosphere increased by 55.8% and 136.7% respectively when sintered at 1150 °C and 1300 °C, compared with those debound in air. The Fe/Ni ratio in $NiFe_2O_4$ phase of the samples debound in N_2 atmosphere was slightly higher than that

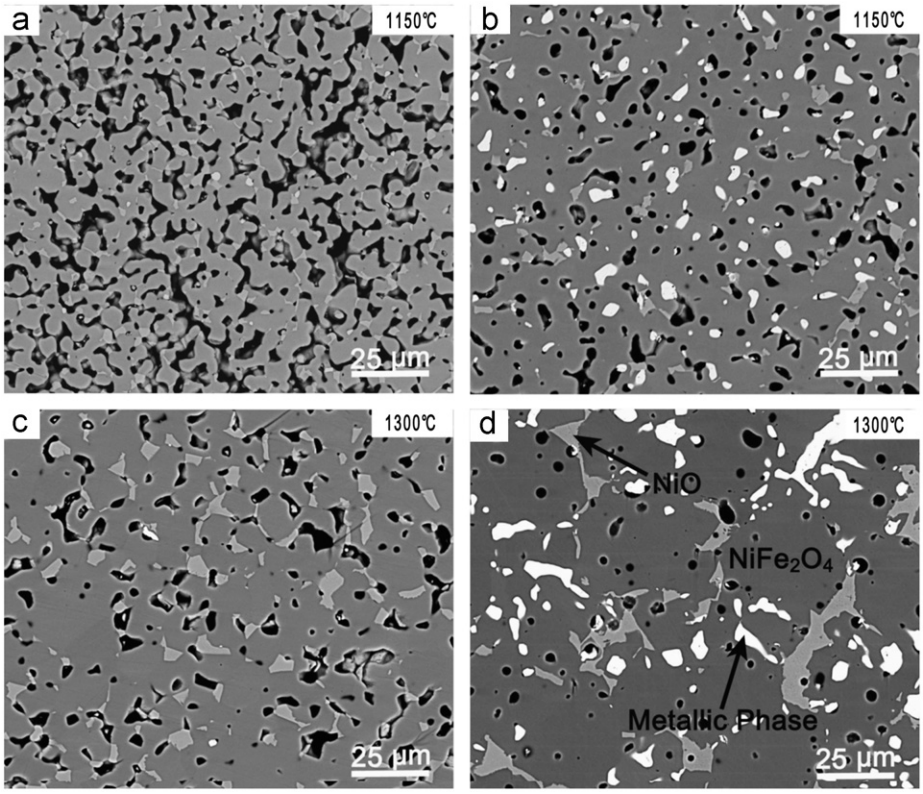

Fig. 4. Micrographs of the samples sintered at 1150 °C and 1300 °C. The binder burnout process of (a) and (c) was performed in air, and that of (b) and (d) were performed in N_2 atmospheres.

Table 1
Densifications, grain sizes of $NiFe_2O_4$, and Fe/Ni atomic ratios in $NiFe_2O_4$ phase of the sintered samples. The binder burnout process was performed in air and N_2 atmospheres respectively.

Sintering temperatures (°C)	Densifications (%)		Grain sizes of $NiFe_2O_4$ (μm)		Fe/Ni atomic ratios in $NiFe_2O_4$ phase	
	in air	in N_2	in air	in N_2	in air	in N_2
1150	79.7	90.7	7.7	12	3.03	3.15
1300	91.1	97.2	12	28.4	3.12	3.79

debound in air when sintered at 1150 °C, while it was much larger at 1300 °C.

The residual carbon contents of the compacts debound in air and N_2 atmospheres were 0.026 wt% and 0.033 wt%, respectively. The Fe^{2+} concentration of $NiFe_2O_4$ sintered in N_2 atmosphere was higher than that sintered in air [15]; therefore the Fe^{2+} concentration of the sample debound in air would increase after sintering in N_2 atmosphere. However, the Fe/Ni atomic ratios in $NiFe_2O_4$ phase shown in Table 1 indicated that the difference of Fe^{2+} concentration still existed in the sintered samples which were treated with different debinding atmospheres. The effect of sintering atmosphere on the increase of Fe^{2+} concentration did not eliminate the influence of debinding atmosphere. Therefore, the effects of the residual carbon and the sintering atmosphere on the differences of sintering densification and growth of ceramic particle could be neglected. The differences should be originated from the debinding atmospheres.

4. Conclusions

In summary, microsized $NiFe_2O_4$ powder was synthesized by molten salt synthesis in KCl flux. The effects of debinding atmosphere on the microstructure and sintering densification of $NiFe_2O_4$ were studied. The surface of $NiFe_2O_4$ particles in the compact containing 1.2 wt% PVA was partially reduced into metallic Ni when the binder burnout process was performed in N_2 atmosphere. The densifications, grain sizes of $NiFe_2O_4$, and Fe/Ni atomic ratios in $NiFe_2O_4$ phase of the sintered sample debound in N_2 atmosphere were much higher than that debound in air when sintered at the same temperature. The N_2 debinding atmosphere was more conducive to the sintering densification and grain growth of $NiFe_2O_4$ compared with air.

Acknowledgments

We acknowledge the financial support from the National Basic Research Program of China (2005CB623703), the Program for New Century Excellent Talents in university of the Ministry of Education of China (no. NCET-08-0572), the National Natural Science Fund for Innovation Group of China (no. 51021063) and the National High-Tech Research and Development Program of China (no. 2008AA030501).

References

[1] J.D. Weyand, S.P. Ray, F.W. Baker, D.H. DeYoung, G.P. Tarcy, Inert Anode for Aluminium Smelting: Final Report for the Period 29 September 1980–30 September 1985, Aluminum Company of America, Washington, DC, 1986.
[2] K.C. Zhou, Y.Q. Tao, Research development of nickel ferrite based cermet inert anode materials, Chinese Journal of Nonferrous Metals 10 (2011) 2418–2429.
[3] R.P. Pawlek, Inert anodes—an update, Aluminium 87 (2011) 77–81.
[4] T.R. Alcorn, A.T. Tabereaux, N.E. Richards, C.F. Windisch Jr, D.M. Strachan, J.S. Gregg, M.S. Frederick, Operational results of pilot cell test with cermet "inert" anodes, in: M.B. Christian (Ed.), Light Metals 1993, TMS, Warrendale, 1993, pp. 433–445.
[5] Z.L. Tian, Y.Q. Lai, Z.Y. Li, J. Li, K.C. Zhou, Y.X. Liu, Cup-shaped functionally gradient $NiFe_2O_4$-based cermet inert anodes for aluminum reduction, Journal of the Minerals Metals and Materials Society 61 (2009) 34–38.
[6] G.P. Tarcy, Corrosion and passivation of cermet inert anodes in cryolite-type electrolytes, in: R.E. Miller (Ed.), Light Metals 1986, TMS, Warrendale, 1986, pp. 309–320.
[7] Y.Q. Lai, X.Z. Li, J. Li, Z.L. Tian, G. Zhang, Y.X. Liu, Effect of metallic phase species on the corrosion resistance of 17 M-(10NiO-$NiFe_2O_4$) cermet inert anode of aluminum electrolysis, Journal of Central South University of Technology 13 (2006) 214–218.
[8] J.D. Weyand, Manufacturing processes used for the production of inert anodes, in: R.E. Miller (Ed.), Light Metals 1986, TMS, Warrendale, 1986, pp. 321–339.
[9] E. Olsen, J. Thonstad, Nickel ferrite as inert anodes in aluminium electrolysis: part I—material fabrication and preliminary testing, Journal of Applied Electrochemistry 29 (1999) 293–299.
[10] B.G. Liu, L. Zhang, K.C. Zhou, Z.Y. Li, H. Wang, Electrical conductivity and molten salt corrosion behavior of spinel nickel ferrite, Solid State Sciences 13 (2011) 1483–1487.
[11] Y.Q. Lai, X.G. Sun, J. Li, H.N. Duan, X.Z. Li, G. Zhang, Z.L. Tian, Densification of Ni–$NiFe_2O_4$ cermets for aluminum electrolysis, Transactions of the Nonferrous Metals Society of China 15 (2005) 666–670.
[12] H.B. He, H.N. Xiao, K.C. Zhou, Effect of additive BaO on corrosion resistance of xCu/(10NiO–$NiFe_2O_4$) cermet inert anodes for aluminum electrolysis, Transactions of the Nonferrous Metals Society of China 21 (2011) 102–108.
[13] J.J. Du, G.C. Yao, Y.H. Liu, J. Ma, G.Y. Zu, Influence of V_2O_5 as an effective dopant on the sintering behavior and magnetic properties of $NiFe_2O_4$ ferrite ceramics, Ceramics International 38 (2012) 1707–1711.
[14] L. Zhang, K.C. Zhou, Z.Y. Li, X.Y. Zhang, Effect of atmosphere on densification in sintering nickel ferrite ceramic for aluminum electrolysis, Chinese Journal of Nonferrous Metals 14 (2004) 1002–1006.
[15] B.G. Liu, K.C. Zhou, Z.Y. Li, D. Zhang, L. Zhang, Microstructure and DC electrical conductivity of spinel nickel ferrite sintered in air and nitrogen atmospheres, Materials Research Bulletin 45 (2010) 1668–1671.
[16] E. Lima Jr, V. Drago, P.F.P. Fichtner, P.H.P. Domingues, Tetrataenite and other Fe–Ni equilibrium phases produced by reduction of nanocrystalline $NiFe_2O_4$, Solid State Communications 128 (2003) 345–350.
[17] J.L. Zhang, J.X. Shi, M.L. Gong, Synthesis of magnetic nickel spinel ferrite nanospheres by a reverse emulsion-assisted hydrothermal process, Journal of Solid State Chemistry 182 (2009) 2135–2140.
[18] J.F. Moulder, W.F. Stickle, P.E Sobol, K.D. Bomben, Handbook of x-ray Photoelectron Spectroscopy: A Reference Book of Standard Spectra for Identification and Interpretation of XPS Data, Perkin–Elmer, Minnesota, US, 1992.